PERGAMON

Computers and Structures 79 (2001) 2009–2027

Computers & Structures

www.elsevier.com/locate/compstruc

A crankshaft system model for structural dynamic analysis of internal combustion engines

Zissimos P. Mourelatos *

Vehicle Analysis and Dynamics Lab, General Motors Research and Development and Planning, Mail Code: 480-106-256, 30500 Mound Road, Warren, MI 48090-9055, USA

Received 14 June 2000; accepted 6 June 2001

Abstract

A system model for analyzing the dynamic behavior of an internal combustion engine crankshaft is described. The model couples the crankshaft structural dynamics, the main bearing hydrodynamic lubrication and the engine block stiffness using a system approach. A two-level dynamic substructuring technique is used to predict the crankshaft dynamic response based on the finite-element method. The dynamic substructuring uses a set of load-dependent Ritz vectors. The main bearing lubrication analysis is based on the solution of the Reynold's equation. Comparison with experimental results demonstrates the accuracy of the model. Numerical results also show the capabilities and significance of the model in engine crankshaft design.

Keywords: Crankshaft–block dynamic interaction; Dynamic substructuring; Journal bearing lubrication; Engine noise, vibration and harshness; Crankshaft design

1. Introduction

Legislative and market pressures on internal combustion engine design call for increased engine power, reduced engine size and improved fuel economy, simultaneously. Also, efforts to reduce engine vibration and radiated noise while improving durability and reliability have become increasingly important to the automotive industry due to more stringent requirements for higher performance, lighter weight, low cost and fast-to-market engine designs. Optimized engine components are therefore required if competitive designs must be realized. Sophisticated analytical tools can greatly enhance the understanding of the physical phenomena associated with the operation of vital engine components. This is particularly true of crankshafts, one of the most analyzed engine components. Many sophisticated crankshaft analysis methods have been reported in the past. This has been mostly facilitated by the use of the finite-element method on high speed computers and the availability of elaborate finite-element preprocessors which can construct complex finite-element mesh models.

In recent years, noise, vibration and harshness (NVH) of automotive engines is becoming an integral part of the design process along with the traditional issues of durability and performance. NVH is strongly related to how customers perceive the quality of the engine; affecting, therefore, its competitiveness in the market place. Extensive static and dynamic analyses have been performed on vital engine components as crankshafts and engine blocks in order to improve their durability [1–4] and NVH performance [5–8]. The engine is a fine-tuned system of individual components. An optimum engine design requires a system approach since the performance of each component can be strongly dependent on the performance of the other components. This is particularly true for the crankshaft–block subsystem [9–12].

A crankshaft–block subsystem consists of the crankshaft and the engine block coupled by the hydrodynamically lubricated main bearings. The loading on the system comes from the cylinder pressure and the

* Tel.: +1-810-986-9212; fax: +1-810-986-0918.
E-mail address: zissimos@gm.com (Z.P. Mourelatos).

0045-7949/01/$ - see front matter
PII: S0045-7949(01)00119-5

piston–connecting rod inertia. The cylinder pressure applied on the piston crown is transmitted to the crankpin through the piston–connecting rod assembly. The inertia of the piston–connecting rod provides a load on the crankpin as well. The crankpin loads deform the crankshaft and are transmitted to the engine block at the main bearing locations through the main bearing hydrodynamics. Both the deformation of the crankshaft and the engine block affect the main bearing film thickness and therefore, the bearing hydrodynamics. For this reason, the mathematical model of the engine system requires three individual models which are coupled together; a structural model of the crankshaft, a structural model of the engine block and a lubrication model of the main bearings.

The large number of studies reported in the literature on the crankshaft–block interaction problem indicates its significance to the industry. A representative sample is given in Refs. [2,10–17]. Due to the complexity of the problem, many simplifying assumptions have been used. The first attempt to solve the problem is reported in Refs. [9,18] where a calculation of bearing performance in statically indeterminate crankshaft systems is described. A static (not dynamic) crankshaft analysis is used and the block elasticity is represented by linear springs. The mobility method [19] describes the oil-film hydrodynamics neglecting, therefore, the important effects of journal misalignment and bearing design attributes as oil grooves and oil holes. The oil-film hydrodynamics have been almost exclusively represented by either the mobility method [10,12–14] or simple spring–damper combinations [15–17]. In some cases the oil-film is completely neglected [11].

The significance of the crankshaft–block interaction problem in internal combustion engine design is due to a variety of reasons. First, the engine crankshaft is a finely optimized component with significant resonances (both torsional and bending) within its normal operating range. These resonances affect, among others, the dynamic stress distribution on crankshafts, bearing caps and engine bulkheads [2,4] and the noise of the engine lower end [3,7,10]. The accurate prediction of dynamic stress levels is important for durability, low weight and high fatigue life [2]. The crankshaft dynamic response is also needed for optimizing crankshaft accessories as pulleys [16,17] and flywheels [4]. Also the consideration of the oil-film hydrodynamics in the crankshaft–block interaction problem provides an enhanced bearing load prediction [4]. This allows for the design of more durable bearings with less friction and therefore, better fuel economy [20,21]. Furthermore, the motion of each journal within the bearing clearance is needed for predicting the magnitude and duration of bearing impacts which normally occur during bearing load reversals. Such a prediction is essential for reducing the emitted noise from the engine lower end [10,22].

This paper describes a crankshaft–block interaction methodology called CRANKSYM (Crankshaft System Model). Section 2 gives an overview of the proposed crankshaft system model where all the features and assumptions are described in detail. Subsequent sections describe the crankshaft structural dynamic analysis and the engine block representation, the developed main bearing hydrodynamic analysis, and the coupled crankshaft–engine block model. The accuracy and efficiency of the crankshaft structural dynamic analysis is demonstrated in Ref. [23]. Comparison with experimental results shows the good accuracy of the proposed methodology. Finally, the capabilities and significance of the proposed crankshaft–engine block system model in engine design are illustrated using a V-shape six-cylinder engine.

2. Overview of the crankshaft system model (CRANKSYM)

CRANKSYM is a system model for analyzing an internal combustion engine crankshaft. In its most general form, it couples the crankshaft structural dynamics, the main bearing hydrodynamic lubrication and the engine block stiffness using a system approach.

A finite-element mesh for the entire crankshaft is needed in order to calculate its structural dynamic response. The main bearing lubrication analysis is performed by solving the 2-D Reynold's equation for each main bearing using the finite-element method. The flexibility of the engine block is represented by its stiffness at each main bearing location. The main output from CRANKSYM is the crankshaft dynamic response in terms of displacements, velocities and accelerations at user specified grid points, natural frequencies and mode shapes, and crankshaft dynamic stresses throughout the engine cycle. The main bearing loads (forces and moments) and bearing performance parameters such as eccentricities, minimum film thickness and maximum film pressure are calculated and output for each bearing. The oil-film thickness and pressure distributions are also calculated at each crankangle throughout the whole engine cycle.

A two-level dynamic substructuring is performed for the structural dynamic analysis of the crankshaft based on load-dependent Ritz vectors which are generated by a subspace algorithm. After the two dynamic reductions, the initial finite-element model size is significantly reduced to very few generalized degrees of freedom which are efficiently integrated in time. The rotating crankshaft is properly coupled with the fixed compliant engine block. The block compliance is represented by a distributed linear elastic foundation at each main bearing location both in the vertical and horizontal planes. This representation accounts not only for the translational

block stiffness but for the rotational block stiffness as well, in both planes. As a result, the bearing loads consist of reaction forces and reaction moments. The reaction moments introduce bearing journal misalignment which is normally neglected in "traditional" lubrication analysis. The stiffness of the elastic foundation can vary around the circumference of each main bearing considering therefore, the anisotropy of the engine block compliance with respect to the crankshaft rotation.

The hydrodynamic analysis of the main bearings is performed by solving the Reynold's equation using the finite-element method. Four journal degrees of freedom are used in the analysis. These are the vertical and lateral translations and rotations of the journal at the middle-bearing location. The rotational degrees of freedom capture the journal misalignment within each main bearing. The robustness of the crankshaft system model is greatly improved with the introduction of a contact algorithm which handles possible touching of a journal with its bearing shell. When the rotational stiffness of the block is considered, the crankshaft may touch the block during part of the engine cycle. This may be due to excessive loading of a bearing, larger than its load carrying capacity.

3. Crankshaft structural dynamic analysis

The crankshaft structural analysis predicts the crankshaft dynamic response based on the finite-element method. A two-level dynamic substructuring with special Ritz vectors is performed. Initially, a given three-dimensional finite-element model of the crankshaft is divided into substructures. Each crankshaft bay and the crankshaft nose and tail (flywheel end) constitute separate substructures. Each substructure is dynamically reduced using a set of load-dependent Ritz vectors. Subsequently, all the substructures are assembled and a second dynamic reduction is performed using a new set of Ritz vectors. A subspace algorithm is used to generate the load-dependent Ritz vectors.

The calculation of eigenvectors for a large structure is computationally expensive. Besides, the participation of a particular eigenvector in the final solution depends on the applied dynamic loading. If the loading frequency is close to a natural frequency of the structure, then the corresponding eigenvector participates significantly in the solution. Furthermore, eigenvectors which are orthogonal to the applied loading do not participate in the solution even if their frequency (corresponding eigenvalue) is contained in the loading. For the above reasons, the eigenvectors may not be the most efficient basis for a dynamic reduction of a complex structure subjected to certain external loading. In this work, special Ritz vectors are used instead of eigenvectors to form the transformation basis for the crankshaft dynamic reduction. It has been demonstrated that use of orthonormal Ritz vectors instead of the same number of eigenvectors, can result in better accuracy in dynamic analysis of complex structures [23–27]. The reason is that the Ritz vectors consider the spatial distribution of the applied loading, whereas the eigenvectors neglect that important information. The first Ritz vector is the static solution to the applied loading. The subsequent Ritz vectors are generated by multiplying the mass matrix by the previous Ritz vector and use the result as a load vector for a new static solution [23,24].

3.1. First level of dynamic substructuring analysis

The dynamic equilibrium equations of the crankshaft modeled using the finite-element method, are written as

$$[M]\{\ddot{U}\} + [C]\{\dot{U}\} + [K]\{U\} = \{F(s,t)\} \tag{1}$$

where $[M]$, $[C]$, $[K]$ and $\{F\}$ are the mass matrix, damping matrix, stiffness matrix and load vector, respectively. The load and displacement (or response) vectors are a function of space (s) and time (t). Eq. (1) can be solved for the displacement vector $\{U\}$.

The crankshaft is divided into a number of substructures by splitting it at the middle of each main bearing location. The initial displacement vector $\{U\}$ of Eq. (1) is partitioned into internal displacements $\{U_i\}$ and retained displacements $\{U_r\}$. The vector $\{U_r\}$ consists of all the displacements of the common interfaces of the substructures plus the displacements of points on the crankshaft centerline at the two ends of each main bearing (Fig. 1). The latter points are used to determine the slope of each main bearing journal. $\{U_i\}$ includes all other displacements in $\{U\}$. Based on this partitioning, the initial displacement vector $\{U\}$ and the mass matrix in Eq. (1) are rewritten as follows:

$$\{U\} = \{\, U_i^1 \quad U_i^2 \quad \cdots \quad |U_r\,\}^T \tag{2}$$

$$[M] = \begin{bmatrix} M_i^1 & 0 & \cdots & M_{ir}^1 \\ 0 & M_i^2 & \cdots & M_{ir}^2 \\ \vdots & \vdots & \ddots & \vdots \\ M_{ir}^{1T} & M_{ir}^{2T} & \cdots & M_r \end{bmatrix} \tag{3}$$

Similar expressions hold for the $[C]$ and $[K]$ matrices and the load vector $\{F\}$. In Eq. (3), the zeros represent null matrices of the appropriate dimensions. Subscripts i and r denote internal and retained degrees of freedom, respectively, and superscripts denote the substructure number or the transpose of a matrix.

The internal displacement vector $\{U_i^\ell\}$ for the ℓth substructure is expressed as

$$\{U_i^\ell\} = [X^\ell]\{u^\ell\} + [T^\ell]\{U_r\} \tag{4}$$

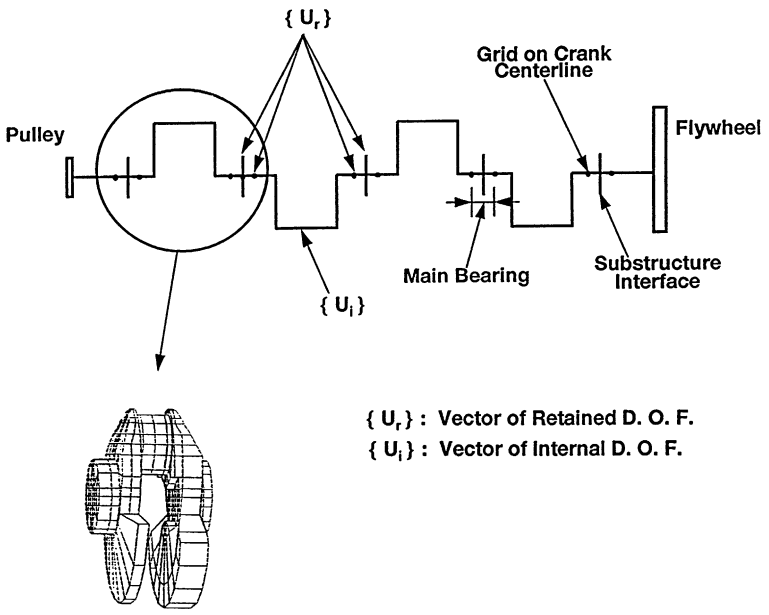

Fig. 1. Some definitions on the crankshaft substructuring.

The transformation matrix $[X^\ell]$ consists of a set of M-orthonormal Ritz vectors calculated with the algorithm of Table 1 based on matrices $\lfloor M_{\mathrm{i}}^\ell \rfloor$, $\lfloor K_{\mathrm{i}}^\ell \rfloor$ and $\lfloor F_{\mathrm{i}}^\ell \rfloor$ for the ℓth substructure. Matrix $\lfloor F_{\mathrm{i}}^\ell \rfloor$ consists of only two spatial load vectors ($k = 2$ in Table 1). The generalized displacement vector $\{u^\ell\}$ is much smaller in size than $\{U_{\mathrm{i}}^\ell\}$. Matrix $\lfloor T^\ell \rfloor$ is the static transformation matrix between the internal displacement vector $\{U_{\mathrm{i}}^\ell\}$ and the retained displacement vector $\{U_{\mathrm{r}}\}$.

Based on Eq. (4), the initial displacement vector $\{U\}$ is transformed as follows:

$$\{U\} = [\Phi]\{\bar{u}\} = \begin{Bmatrix} U_{\mathrm{i}}^1 \\ \vdots \\ U_{\mathrm{i}}^\ell \\ \vdots \\ --- \\ U_{\mathrm{r}} \end{Bmatrix} = \begin{bmatrix} X^1 & \cdots & 0 & \cdots & \vdots & T^1 \\ \vdots & & \vdots & & \vdots & \vdots \\ 0 & \cdots & X^\ell & \cdots & \vdots & T^\ell \\ \vdots & & \vdots & & \vdots & \vdots \\ -- & -- & -- & -- & -- & -- \\ 0 & \cdots & 0 & \cdots & \vdots & I \end{bmatrix} \begin{Bmatrix} u^1 \\ \vdots \\ u^\ell \\ \vdots \\ --- \\ U_{\mathrm{r}} \end{Bmatrix} \tag{5}$$

Application of Eq. (5) transformation to Eq. (1) results in the following reduced dynamic system:

$$[\overline{M}]\{\ddot{\bar{u}}\} + [\overline{C}]\{\dot{\bar{u}}\} + [\overline{K}]\{\bar{u}\} = \{\overline{F}\} \tag{6}$$

where

$$[\overline{M}] = [\Phi]^{\mathrm{T}}[M][\Phi] = \begin{bmatrix} \overline{M}_{\mathrm{i}}^1 & \cdots & 0 & \cdots & \overline{M}_{\mathrm{ir}}^1 \\ \vdots & & \vdots & & \vdots \\ 0 & \cdots & \overline{M}_{\mathrm{i}}^\ell & \cdots & \overline{M}_{\mathrm{ir}}^\ell \\ \vdots & & \vdots & & \vdots \\ \overline{M_{\mathrm{ir}}^1}^{\mathrm{T}} & \cdots & \overline{M_{\mathrm{ir}}^\ell}^{\mathrm{T}} & \cdots & \overline{M}_{\mathrm{r}} \end{bmatrix} \tag{7a}$$

$$\overline{M}_{\mathrm{i}}^\ell = X^{\ell\mathrm{T}} M_{\mathrm{i}}^\ell X^\ell \tag{7b}$$

$$\overline{M}_{\mathrm{ir}}^\ell = X^{\ell\mathrm{T}}(M_{\mathrm{i}}^\ell T^\ell + M_{\mathrm{ir}}^\ell) \tag{7c}$$

$$\overline{M}_{\mathrm{r}} = M_{\mathrm{r}} + \sum_\ell (T^{\ell\mathrm{T}} M_{\mathrm{i}}^\ell T^\ell + M_{\mathrm{ir}}^{\ell\mathrm{T}} T^\ell + T^{\ell\mathrm{T}} M_{\mathrm{ir}}^\ell) \tag{7d}$$

Similar expressions hold for $\overline{C}$ and $\overline{K}$. The reduced load vector $\{\overline{F}\}$ is given by

$$\{\overline{F}\} = \{\, \overline{F_{\mathrm{i}}^1} \quad \cdots \quad \overline{F_{\mathrm{i}}^\ell} \quad \cdots \quad \overline{F_{\mathrm{r}}} \,\}^{\mathrm{T}} \tag{8a}$$

where

$$\overline{F}_{\mathrm{i}}^\ell = X^\ell F_{\mathrm{i}}^\ell \tag{8b}$$

and

$$\overline{F}_{\mathrm{r}} = F_{\mathrm{r}} + \sum_\ell T^\ell F_{\mathrm{i}}^\ell \tag{8c}$$

More information about the crankshaft dynamic substructuring process and the load-dependent Ritz vector transformation can be found in Ref. [23].

Table 1
A subspace algorithm to calculate load-dependent Ritz vectors

1.	*Given input matrices*
	$[M]$: mass matrix $(n \times n)$
	$[K]$: stiffness matrix $(n \times n)$
	$[F]$: block of k independent spatial load vectors $(n \times k)$
2.	*Triangularize stiffness matrix*
	$[K] = [L]^{\mathrm{T}}[D][L]$
3.	*Solve for initial static block* $[X_1]$
	a. Solve for block $[x^*] = [x_1^*, x_2^*, \ldots, x_k^*]$
	$[K][x^*] = [F]$
	b. Get block $[\overline{X}] = [\bar{x}_1, \bar{x}_2, \ldots, \bar{x}_k]$ by M-normalization of vectors $\{x_j^*\}$, $j = 1, 2, \ldots, k$
	$\{x_j^*\}^{\mathrm{T}}[M]\{x_j^*\} = a$
	$\{\bar{x}_j\} = a^{-1/2}\{x_j^*\}$
	c. Get block $[\hat{X}] = [\hat{x}_1, \hat{x}_2, \ldots, \hat{x}_k]$ by M-orthogonalization of vectors in $[\overline{X}]$.
	Repeat for $j = 2, 3, \ldots, k$:
	$[C_j] = [\bar{x}_1, \bar{x}_2, \ldots, \bar{x}_{j-1}]^{\mathrm{T}}[M]\{\bar{x}_j\}$
	$\{\hat{x}_j\} = \{\bar{x}_j\} - [\bar{x}_1, \bar{x}_2, \ldots, \bar{x}_{j-1}][C_j]$
	d. M-normalize block $[\hat{X}]$
	$[\hat{X}]^T[M][\hat{X}] = [\Lambda]$
	$[X_1] = [\hat{X}][\Lambda]^{-1/2}$
4.	*Solve for subsequent blocks* $[X_i]$, $i = 2, 3, \ldots, p$
	a. Solve for block $[X_i^*]$
	$[K][X_i^*] = [M][X_{i-1}]$
	b. Get block $[\hat{X}_i]$ by M-orthogonalization of $[X_i^*]$ against all previous blocks
	$[C] = [[X_1], \ldots, [X_{i-1}]]^{\mathrm{T}}[M][X_i^*]$
	$[\hat{X}_i] = [X_i^*] - [[X_1], \ldots, [X_{i-1}]][C]$
	c. Get block $[\overline{X}_i]$ by M-orthogonalization of $[\hat{X}_i]$ against all previous blocks according to Step 4b.
	d. Get block $[X_i]$ by M-orthogonalization of block $[\overline{X}_i]$ according to Steps 3c and 3d.

3.2. Second level of dynamic substructuring analysis

The reduced displacement vector $\{\bar{u}\}$ in Eq. (5) contains the retained displacement vector $\{U_r\}$ which can be of a fairly large size. For this reason, a second level of substructuring is performed which further reduces the number of retained degrees of freedom.

The vector $\{U_r\}$ is partitioned as

$$\{{}_1U_r\} = \{\, {}_2U_i \quad {}_2U_r \,\}^{\mathrm{T}} \tag{9}$$

where the left subscript indicates the level of substructuring analysis. $\{{}_2U_r\}$ contains the displacements of three points at the left end, middle and right end of each main bearing on the crankshaft centerline. $\{{}_2U_i\}$ includes all the other displacements of the substructure interfaces which were retained in the first level of substructuring. Due to the partitioning of Eq. (9), the reduced displacement vector $\{\bar{u}\}$ becomes

$$\{{}_1\bar{u}\} = \{\, {}_2u_i \quad {}_2U_r \,\}^{\mathrm{T}} \tag{10a}$$

where

$$\{{}_2u_i\} = \{\, {}_1u^1 \quad \cdots \quad {}_1u^\ell \quad \cdots \quad {}_2U_i \,\}^{\mathrm{T}} \tag{10b}$$

The reduced matrices $[\overline{M}]$, $[\overline{C}]$ and $[\overline{K}]$ and the load vector $\{\overline{F}\}$ from the first level of substructuring are partitioned according to Eqs. (10a) and (10b), and the process described in the previous paragraph is repeated. A new Ritz transformation matrix $[X]$ is calculated using again the algorithm of Table 1, and a new reduced system, similar to that of Eq. (6), is formed.

It has been found through extensive applications of the proposed method to a variety of automotive crankshafts, that 20 Ritz vectors are enough for both levels of substructuring. Although the number of Ritz vectors is arbitrary, 15–20 Ritz vectors are usually enough to obtain good accuracy in calculating the dynamic response of a crankshaft. A larger number can be also tried until there is no improvement in the calculated dynamic response.

After the two reductions, the reduced model consists of approximately 50–100 degrees of freedom only. This translates to substantial computational savings in performing a crankshaft dynamic analysis. The computational savings become even more important when the crankshaft dynamic analysis is coupled with the main bearing hydrodynamics to find the combined system response.

The two-level dynamic substructuring analysis and the algorithm to find the Ritz vectors (Table 1) have been implemented in the general purpose program MSC/NASTRAN [28] using DMAP ALTERS [29]. Due to the excellent data management capabilities and efficient matrix operations of MSC/NASTRAN, the potentially

very large stiffness and mass matrices as well as a variety of other auxiliary large matrices are handled very efficiently. Initially, MSC/NASTRAN calculates the mass and stiffness matrices of the model. Then two separate DMAP ALTERS, instruct MSC/NASTRAN to implement the Ritz vector algorithm of Table 1 for the two levels of substructuring. In the process, the DMAP ALTERS perform a number of data manipulation tasks such as partition and multiplication of large matrices, assembling of data from different substructures, solution of linear systems of equations, etc. This not only solves the problem of managing very large matrices but also reduces the overall computational effort since MSC/NASTRAN performs the bulk of the computations very efficiently.

3.3. Crankshaft loading

The crankshaft is mainly loaded by the engine operating load which comes from the cylinder combustion. This load is transmitted through the piston and connecting rod to the crankpin of the crankshaft. The piston and the connecting rod are treated as rigid bodies and their inertia loads are calculated and combined with the combustion load. The combined load is applied on the crankpin in the rotating coordinate system. The belt loads are also applied on the crankshaft.

Since the analysis is performed in the rotating coordinate system, the crankshaft inertia load due to centrifugal forces is also applied on the crankshaft. For a particular finite-element model of the crankshaft, this inertia load is equal to $mr\omega^2$, where m is the mass of the finite element, r the distance of its center of gravity from the crankshaft rotation axis and ω the crankshaft rotational velocity. This load is commonly known as "WR segment" loading. The coriolis forces are neglected.

3.4. Structural damping

Rayleigh damping is used to represent the crankshaft structural damping. The damping matrix $[\overline{C}]$ in Eq. (6) is taken as

$$[\overline{C}] = \alpha[\overline{K}] + \beta[\overline{M}] \tag{11}$$

where α and β are two constants to be determined from two specified damping ratios which correspond to two unequal natural frequencies of the system. It has been shown [30] that if the system eigenvectors are $[C]$-orthogonal, the following equation holds

$$\beta + \alpha\omega_i^2 = 2\varsigma_i\omega_i \tag{12}$$

where ω_i is the ith natural frequency of the system and ζ_i is the damping ratio for the ith mode. Given the natural frequencies and damping ratios of two different modes, the coefficients α and β can be determined by solving Eq. (12). Subsequently, Eq. (12) can be used to calculate ζ_i at any frequency ω_i. The Rayleigh damping is a computationally convenient way to approximate the actual structural damping.

3.5. Crankshaft bent and engine block misboring

Crankshaft "bent" (Fig. 2a) and engine block misboring (Fig. 2b) represent manufacturing imperfections.

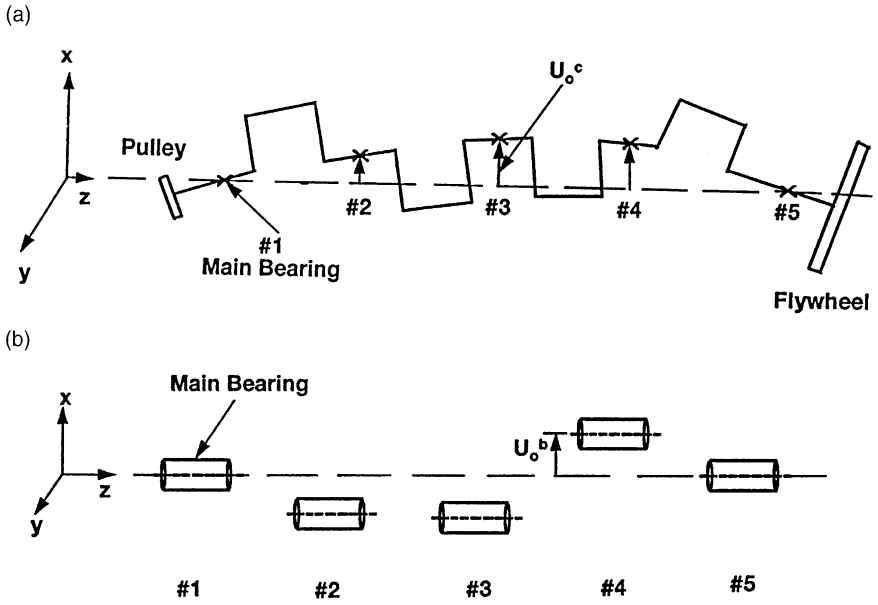

Fig. 2. (a) Schematic of crankshaft "bent". (b) Schematic of engine block misboring.

The forging, heat treating and machining operations necessary to produce a crankshaft, sometimes produce a slightly bent crankshaft. Since this effect is expected, the crankshaft is subsequently straightened so that it conforms to certain finished tolerances. However, it is very difficult to perfectly straighten the crankshaft. Similarly, the main bearing bores in the block structure may lie on different centerlines due to slight misboring. Since the crankshaft bent and the engine block misboring can induce significant loading on the main bearings, they are both included in the formulation of the crankshaft–engine block system model.

4. Representation of engine block

The crankshaft is supported by the engine block at the main bearing locations. In this work the engine block is represented by its static stiffness neglecting therefore the engine block dynamic behavior. The engine block stiffness can be represented by a vertical and horizontal value for each main bearing. In practice, the vertical and horizontal stiffnesses are always different and they both vary around the circumference of each main bearing.

The engine block support can be modeled by a concentrated stiffness at mid-bearing position or by a distributed stiffness along the bearing length. In the former case, the bearing loads consist of reaction forces only. If these loads are used in a traditional main bearing lubrication analysis, there will be no journal misalignment. However, dynamic misalignment can have a significant influence on the main bearing performance. The issue of dynamic misalignment can be of concern with the increasing number of four-cylinder long stroke engines and V6 configurations where adequate main bearing performance remains a design challenge.

The journal misalignment can be calculated by modeling the engine block flexibility with a distributed stiffness along the bearing length (Fig. 3a). In this study, three linear springs are used along the bearing length (one spring at each bearing end and one spring at the mid-bearing location) to represent the distributed engine block flexibility in both the vertical and horizontal planes (Fig. 3b). This representation accounts for the translational and rotational engine block stiffness. As a result, the bearing loads consist of reaction forces and reaction moments. If the translational bearing stiffness is k, the three springs have stiffnesses $k/6$, $2k/3$ and $k/6$ (Fig. 3b). These stiffnesses have been calculated so that the translational and the rotational bearing stiffnesses with respect to the mid-bearing location are the same between the distributed block stiffness and the equivalent distributed block stiffness models.

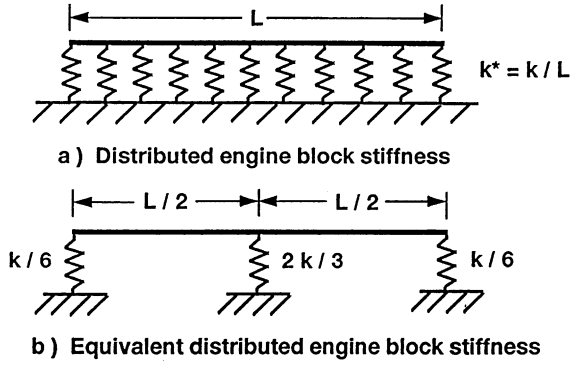

Fig. 3. Representation of the engine block stiffness.

At each time step during the dynamic simulation of the crankshaft motion, the reaction of each main bearing depends on the local engine block stiffness which, in turn, depends on the circumferential location of the resultant main bearing reaction. Therefore, a nonlinear solver must iterate between assumed local engine block stiffnesses for each bearing and the resulting main bearing reactions until it calculates the latter with reasonable accuracy. For computational efficiency, the main bearing reaction from the previous time step is used in this work to estimate the local engine block stiffness needed at the current time step. This feature constitutes a unique engine block stiffness representation which fully accounts for the anisotropy of the engine block flexibility as seen by a rotating crankshaft. The coupling stiffness between the vertical and horizontal planes of the same bearing has been neglected. The coupling stiffness among different bearings has also been neglected.

5. Main bearing hydrodynamic analysis

The crankshaft structure is supported by the oil-film hydrodynamic pressure of the main bearings. The oil-film pressure distribution is described by the Reynolds equation which is derived from the Navier–Stokes equations and the continuity equation under simplifying assumptions [31]. For a Newtonian fluid, the Reynolds equation is written as

$$\frac{\partial}{\partial z}\left(h^3\frac{\partial p}{\partial z}\right)+\frac{1}{R^2}\frac{\partial}{\partial \theta}\left(h^3\frac{\partial p}{\partial \theta}\right)=6\mu\omega\frac{\partial h}{\partial \theta}+12\mu\frac{\partial h}{\partial t} \qquad (13)$$

where $p(z,\theta,t)$ is the oil-film pressure, $h(z,\theta,t)$ is the oil-film thickness, μ is the oil viscosity, R is the journal radius and ω is the crankshaft angular velocity. The bearing coordinate system and notation are shown in Fig. 4. The first and second terms of the right-hand side of Eq. (13) represent the shear or wedge film effect and the oil squeeze film effect, respectively.

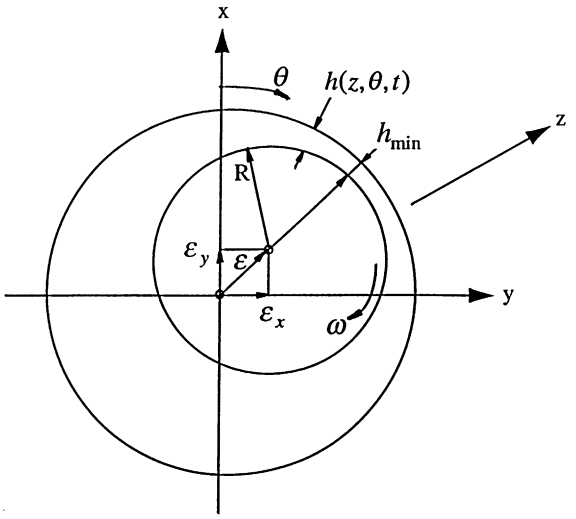

Fig. 4. Bearing coordinate system and notation.

There is a prescribed pressure p_h along the oil grooves and a prescribed pressure p_a at the two bearing ends

$$p(z,\theta,t) = \begin{cases} p_h & \text{on} \quad \Gamma_1 \\ p_a & \text{on} \quad \Gamma_2 \end{cases} \tag{14}$$

where Γ_1 and Γ_2 denote the oil-film domains with specified pressure. The oil-film pressure distribution can be obtained by solving the Reynolds equation (13) subjected to the boundary conditions of Eq. (14). The solution however will give negative pressure in the cavitated region downstream circumferentially from the line of minimum film thickness $h_{\min}$ (see Fig. 4). For this reason, a cavitation boundary condition must be used in solving Eq. (13) in order to obtain a meaningful oil-film pressure distribution.

There are many cavitation conditions used in the literature. The simplest is the Half Sommerfeld cavitation condition in which positive pressures extend through half the bearing circumference and the other half is regarded as cavitated [31]. Another cavitation condition is the Gümbel condition in which the Reynolds equation (13) is first solved subjected to the specified pressures of Eq. (14) and then the cavitation region is determined by disallowing the existence of subambient pressures. A more accurate cavitation condition is the Reynolds or Swift–Stieber condition which requires the pressure gradient to be zero and the pressure to be equal to the cavitation pressure at the cavitation boundary. This condition ensures mass flow continuity at the rupture boundary but not at the reformation boundary [32,33]. It is adequate for determining load capacity, or alternatively, minimum film thickness and journal orbit under dynamic loading provided that the oil film is isothermal and there is oil availability [33]. The most accurate cavitation condition is the Jakobsson-Floberg and Olsson (JFO) condition which conserves mass both at the rupture and the reformation boundaries [32,33]. Comparisons between the Reynolds and JFO conditions have shown that the former is adequate for bearing load capacity calculations while the latter is needed to predict accurately the oil flow in the bearing [33].

Although the Reynolds equation (13) is linear, when the Reynolds or JFO cavitation conditions are used, the problem of determining the oil pressure distribution becomes nonlinear since the cavitation region is not known a priori. This can increase the computational cost substantially. It is estimated [34] that in a dynamically loaded bearing the use of the Reynolds cavitation condition may increase the computational cost by at least 50%. The Gümbel cavitation condition relaxes the zero-pressure gradient requirement and is therefore, a compromise to the Reynolds condition. Although it is unacceptable for oil flow prediction, it introduces an error of only about 5% in calculating the bearing load capacity [34,35]. In the present crankshaft system model, the oil-film hydrodynamic pressure couples the crankshaft dynamic motion with the engine block static motion. The oil-film hydrodynamic pressure depends on the oil-film thickness which is defined by the crankshaft orbit within the bearing. Thus, a relatively accurate calculation of the oil-film pressure and the journal orbit is needed. On the other hand for practical purposes, the computational cost in performing a coupled analysis between the crankshaft dynamics and oil-film hydrodynamics must be kept low. Based on this reasoning, the Gümbel cavitation condition is used in the present work since it provides acceptable accuracy in oil-film pressure calculations with minimum computational cost.

5.1. Linear perturbation approach

At a particular time (or crankangle) during the engine cycle, the relative position of the journal within the bearing defines the oil-film thickness h. Based on the oil-film thickness, the corresponding film pressure p is calculated by solving the Reynolds equation (13). Subsequently, p is integrated around the journal to get the bearing load capacity. In this work, the so-called inverse lubrication problem must be solved repeatedly as it will be illustrated later in this report. At time t, the film thickness $h(z,\theta,t)$ is calculated in an iterative manner until the corresponding load capacity matches a given applied load.

If the calculation time step Δt is relatively small, both the film thickness $h(z,\theta,t)$ and the corresponding oil-film pressure distribution $p(z,\theta,t)$, or equivalently the load capacity, will differ from the previous time $t-\Delta t$ by a small amount Δh and Δp, respectively. This constitutes the basis of a linear perturbation approach to solve the Reynolds equation (13). A similar approach has been

used in Ref. [36] to calculate the dynamic coefficients of a journal bearing.

At a particular time t, the following assumption is made

$$h(z,\theta,t) = h_0 + \Delta h, \text{ and}$$
$$p(z,\theta,t) = p_0 + \Delta p \tag{15}$$

where $h_0 = h(z,\theta,t-\Delta t)$ and $p_0 = p(z,\theta,t-\Delta t)$. Substitution of Eq. (15) into Eq. (13), retention of only the first order terms and separation of variables yields the following two equations

$$\frac{\partial}{\partial z}\left(h_0^3\frac{\partial p_0}{\partial z}\right)+\frac{1}{R^2}\frac{\partial}{\partial\theta}\left(h_0^3\frac{\partial p_0}{\partial\theta}\right) = 6\mu\omega\frac{\partial h_0}{\partial\theta}+12\mu\frac{\partial h_0}{\partial t} \tag{16a}$$

$$\frac{\partial}{\partial z}\left(h_0^3\frac{\partial \Delta p}{\partial z}\right)+\frac{1}{R^2}\frac{\partial}{\partial\theta}\left(h_0^3\frac{\partial \Delta p}{\partial\theta}\right) = -\frac{\partial}{\partial z}\left(3h_0^2\Delta h\frac{\partial p_0}{\partial z}\right)-\frac{1}{R^2}\frac{\partial}{\partial\theta}\left(3h_0^2\Delta h\frac{\partial p_0}{\partial\theta}\right) + 6\mu\omega\frac{\partial\Delta h}{\partial\theta}+12\mu\frac{\partial\Delta h}{\partial t} \tag{16b}$$

Both Eqs. (16a) and (16b) will be solved using the finite-element method. The weak (or variational) formulation and the discretization of the oil-film domain using a bilinear rectangular element are described in the following sections.

5.2. Weak formulation

The Galerkin method or weighted residuals method is used to obtain the variational, or weak, form of Eqs. (16a) and (16b). Eq. (16a) is multiplied by a virtual nominal pressure $\bar{p}_0$ and Eq. (16b) is multiplied by a virtual perturbation pressure $\Delta\bar{p}$. Subsequently both equations are integrated over the oil-film domain Ω. Integration by parts yields the following weak forms for Eqs. (16a) and (16b), respectively

$$\int_\Omega h_0^3\frac{\partial p_0}{\partial z}\frac{\partial\bar{p}_0}{\partial z}\,d\Omega+\frac{1}{R^2}\int_\Omega h_0^3\frac{\partial p_0}{\partial\theta}\frac{\partial\bar{p}_0}{\partial\theta}\,d\Omega = \int_\Omega 6\mu\omega h_0\frac{\partial\bar{p}_0}{\partial\theta}d\Omega-\int_\Omega 12\mu\frac{\partial h_0}{\partial t}\bar{p}_0 d\Omega \tag{17a}$$

$$\int_\Omega h_0^3\frac{\partial\Delta p}{\partial z}\frac{\partial\Delta\bar{p}}{\partial z}d\Omega+\frac{1}{R^2}\int_\Omega h_0^3\frac{\partial\Delta p}{\partial\theta}\frac{\partial\Delta\bar{p}}{\partial\theta}d\Omega = -\int_\Omega 3h_0^2\frac{\partial p_0}{\partial z}\Delta h\frac{\partial\Delta\bar{p}}{\partial z}d\Omega-\frac{1}{R^2}\int_\Omega 3h_0^2\frac{\partial p_0}{\partial\theta}\Delta h\times\frac{\partial\Delta\bar{p}}{\partial\theta}d\Omega+\int_\Omega 6\mu\omega\Delta h\frac{\partial\Delta\bar{p}}{\partial\theta}d\Omega-\int_\Omega 12\mu\frac{\partial\Delta h}{\partial t}\Delta\bar{p}\,d\Omega \tag{17b}$$

All the boundary terms from the integration by parts are zero since the pressure is specified on the boundaries according to Eq. (14).

5.3. Discretization of oil-film domain using a bilinear rectangular element

The discretization of the two-dimensional oil-film domain is commonly done using linear triangular elements [37,38]. In this work however, a bilinear rectangular element with "hourglass control" is adopted due to its superior computational efficiency without loss of accuracy.

The "hourglass control" technique was first introduced in Ref. [39]. It is a reduced integration technique used to form element stiffness matrices with a small computational effort without great loss of accuracy in the finite-element approximations. Reduced integration techniques, using lower quadrature rules, are known to be computationally efficient. However, they result in a singular global stiffness matrix for certain boundary conditions due to the existence of hourglass (zero energy) modes. To avoid the singularity, one can use either a higher quadrature rule in at least one element, or provide external restraints. The hourglass control method with a higher quadrature rule can be utilized to eliminate the singularity [39,40]. The method was first applied to lubrication problems in Ref. [41].

The complete derivation of the bilinear rectangular oil-film element with hourglass control is presented in Ref. [42]. The element fluidity matrix and the load vector are derived for an oil-film element. The two-dimensional oil-film domain is discretized using a uniform grid of rectangular elements. Each rectangular element has dimensions $(\Delta z,\Delta\theta)$. After the calculation of the integrals in the weak formulations, the element equations for the nominal and perturbation pressure respectively are as follows [42]:

$$\lfloor K^e\rfloor\{\underline{p_0}\}_e = \{f_0^e\} \tag{18a}$$

$$\lfloor K^e\rfloor\{\Delta\underline{p}\}_e = \{f_1^e\} \tag{18b}$$

where the element fluidity matrix $[K^e]$ and the element load vectors $\{f_0^e\}$ and $\{f_1^e\}$ are

$$[K^e] = \frac{(h_0^e)^3}{R^2}\frac{\Delta z}{4\Delta\theta}\frac{1}{3}\begin{bmatrix}4&2&-2&-4\\2&4&-4&-2\\-2&-4&4&2\\-4&-2&2&4\end{bmatrix} + (h_0^e)^3\frac{\Delta\theta}{4\Delta z}\frac{1}{3}\begin{bmatrix}4&-4&-2&2\\-4&4&2&-2\\-2&2&4&-4\\2&-2&-4&4\end{bmatrix} \tag{19}$$

$$\{f_0^e\} = 3\mu\omega h_0^e \Delta z \begin{Bmatrix} -1 \\ -1 \\ 1 \\ 1 \end{Bmatrix} - 3\mu \left(\frac{\partial h_0}{\partial t} \right)^e \Delta\theta \Delta z \begin{Bmatrix} 1 \\ 1 \\ 1 \\ 1 \end{Bmatrix} \tag{20a}$$

$$\{f_1^e\} = \left[6\mu\omega - \frac{3(h_0^e)^2}{R^2} \frac{\partial p_0}{\partial \theta} \right] \Delta h^e \frac{\Delta z}{2} \begin{Bmatrix} -1 \\ -1 \\ 1 \\ 1 \end{Bmatrix} - 3(h_0^e)^2 \frac{\partial p_0}{\partial z} \Delta h^e \frac{\Delta\theta}{2} \begin{Bmatrix} -1 \\ 1 \\ 1 \\ -1 \end{Bmatrix} - 3\mu \frac{\partial(\Delta h^e)}{\partial t} \Delta\theta \Delta z \begin{Bmatrix} 1 \\ 1 \\ 1 \\ 1 \end{Bmatrix} \tag{20b}$$

Notice that the fluidity matrix for each element can be calculated by simply multiplying two constant matrices which are common for *all* elements, by the cubic power of an average element film thickness $(h_0^e)^3$. Similarly the load vectors for each element (Eqs. (20a) and (20b)) are calculated by multiplying constant vectors, again common among all elements, by the average element film thickness or the average element squeeze film rate. The calculation and assembly time for the global fluidity matrix is, therefore, greatly shortened. The resulting computational savings compared to the traditional linear triangular element used in Ref. [38] is about 40% [41]. In addition, due to the linear perturbation approach, the fluidity matrix $[K^e]$ is common in Eqs. (18a) and (18b). Thus it has to be calculated only once at each time step resulting in substantial computational savings. Finally, the element equations (18a) and (18b) are assembled over all elements of the oil domain to get the corresponding global equations:

$$[K]\{\underline{p_0}\} = \{f_0\} \tag{21a}$$

and

$$[K]\{\Delta\underline{p}\} = \{f_1\} \tag{21b}$$

At each time step, Eq. (21a) is solved once for the nominal film pressure p_0 and Eq. (21b) is solved repeatedly for Δp by varying Δh, until the total pressure $p = p_0 + \Delta p$ supports the applied load (inverse lubrication problem). A modified version of Newton's method is used for this nonlinear iteration to calculate the correct Δh at each time step.

Since the lubrication model in this work is coupled with the crankshaft and engine block structural models, its computational efficiency (without compromising the accuracy) allows the system model to be a useful practical design tool. The combination of the linear perturbation approach and the hourglass control technique ensure the computational efficiency of the lubrication analysis with minimal loss of accuracy. The accuracy and efficiency of the lubrication model is demonstrated in Ref. [42].

6. Coupled crankshaft–engine block model

The reduced crankshaft model is described in the rotating coordinate system by

$$[M^c]\{\ddot{u}^c\} + [C^c]\{\dot{u}^c\} + [K^c]\{u^c\} = \{F^c\} \tag{22}$$

The vector $\{u^c\}$ is partitioned as

$$\{u^c\} = \{u_i^c || U_r^c\}^T \tag{23}$$

where $\{u_i^c\}$ is the generalized displacement vector after the second level of substructuring, $\{U_r^c\}$ is the crankshaft retained (subscript r) displacement vector, and $\{F^c\}$ is the vector of applied forces on the crankshaft. The superscript c, in the above quantities, denotes the crankshaft.

The engine block model is described in the rotating coordinate system by

$$[C^b]\{\dot{U}_r^b\} + [K^b]\{U_r^b\} = \{F^b\} \tag{24}$$

where $\{U_r^b\}$ is the block retained (subscript r) displacement vector, and $\{F^b\}$ is the vector of applied forces on the block. The superscript b in the above quantities, denotes the block.

The mass inertia effect is neglected for the block model. The block stiffness matrix $[K^b]$ is given in the rotating coordinate system as follows

$$[K^b] = [T]^T \begin{bmatrix} k_X & 0 \\ 0 & k_Y \end{bmatrix} [T] = \begin{bmatrix} k_x & k_{xy} \\ k_{yx} & k_y \end{bmatrix} \tag{25}$$

where

$$[T] = \begin{bmatrix} \cos\theta & -\sin\theta \\ \sin\theta & \cos\theta \end{bmatrix} \tag{26}$$

and

$$k_x = k_X \cos^2\theta + k_Y \sin^2\theta \tag{27a}$$

$$k_y = k_X \sin^2\theta + k_Y \cos^2\theta \tag{27b}$$

$$k_{xy} = k_{yx} = (k_Y - k_X)\sin\theta\cos\theta \tag{27c}$$

The angle of rotation θ is measured clockwise from the vertical position. The block damping matrix $[C^b]$ is defined similarly. Inclusion of the block damping is necessary because it dampens any crankshaft free-body motion.

Let

$$\{U_T^c\} = \{U_o^c\} + \{U_r^b\} \tag{28a}$$

$$\{U_T^b\} = \{U_o^b\} + \{U_r^b\} \tag{28b}$$

U_T^c, U_T^b are the total (subscript T) displacements of the crankshaft and block respectively, relative to a straight reference line at the mains (Fig. 2), including elastic deformation.

U_o^c, U_o^b are the crankshaft "bent" and engine block misboring, respectively. They are known deviations or offsets (subscript o) from the same reference line.

U_r^c, U_r^b are the crankshaft and block retained displacement vectors, respectively. They represent the elastic deformation of the crankshaft and block from their undeformed position.

All the above vectors include the crankshaft and block displacements at the left end, middle position and right end of each main bearing. The reference line needed to define the vectors is arbitrarily taken as a straight line passing through the middles of the first (fan end) and the last (flywheel) bearings. The offsets of the first and last bearings are arbitrarily set to zero. The "run-out" of the other bearings, or the amount each bearing deviates from that straight line in the rotating crankshaft coordinate system, is then entered as offset. The engine block misboring is specified in a similar way but in the fixed coordinate system.

Based on the partitioning of Eq. (23), Eq. (22) can be written as

$$\begin{bmatrix} M_{ii}^c & M_{ir}^c \\ M_{ir}^{cT} & M_{rr}^c \end{bmatrix} \begin{Bmatrix} \ddot{u}_i^c \\ \ddot{U}_r^c \end{Bmatrix} + \begin{bmatrix} C_{ii}^c & C_{ir}^c \\ C_{ir}^{cT} & C_{rr}^c \end{bmatrix} \begin{Bmatrix} \dot{u}_i^c \\ \dot{U}_r^c \end{Bmatrix} + \begin{bmatrix} K_{ii}^c & K_{ir}^c \\ K_{ir}^{cT} & K_{rr}^c \end{bmatrix} \begin{Bmatrix} u_i^c \\ U_r^c \end{Bmatrix} = \begin{Bmatrix} F_i^c \\ F_r^c \end{Bmatrix} \tag{29}$$

The bearing eccentricity is defined as the difference of the total displacements of the crankshaft and block at the bearing locations; i.e.

$$\{\varepsilon\} = \{U_T^c\} - \{U_T^b\} \tag{30}$$

or due to Eqs. (28a) and (28b)

$$\{U_r^b\} = \{U_o^c\} - \{U_o^b\} + \{U_r^c\} - \{\varepsilon\} \tag{31}$$

Also due to action and reaction,

$$\{F_r^c\} = -\{F^b\} \tag{32}$$

Combining Eqs. (24), (31) and (32) yields

$$\{F_r^c\} = [C^b](\{\dot{\varepsilon}\} + \{\dot{U}_o^b\} - \{\dot{U}_o^c\}) + [K^b](\{\varepsilon\} + \{U_o^b\} - \{U_o^c\}) - [C^b]\{\dot{U}_r^c\} - [K^b]\{U_r^c\} \tag{33}$$

Since the crankshaft "bent" $\{U_o^c\}$ is a vector of constants in the rotating coordinate system, $\{\dot{U}_o^c\}$ is always equal to zero. However, since the block misboring $\{U_o^b\}$ is given in the fixed coordinate system, it must be transformed to the rotating coordinate system using Eq. (26). Due to that transformation, $\{\dot{U}_o^b\}$ is not zero unless the block misboring has the same value in the vertical and horizontal directions at each bulkhead location. Substitution of Eq. (33) in Eq. (29) gives:

$$\begin{bmatrix} M_{ii}^c & M_{ir}^c \\ M_{ir}^{cT} & M_{rr}^c \end{bmatrix} \begin{Bmatrix} \ddot{u}_i^c \\ \ddot{U}_r^c \end{Bmatrix} + \begin{bmatrix} C_{ii}^c & C_{ir}^c \\ C_{ir}^{cT} & C_{rr}^c + C^b \end{bmatrix} \begin{Bmatrix} \dot{u}_i^c \\ \dot{U}_r^c \end{Bmatrix} + \begin{bmatrix} K_{ii}^c & K_{ir}^c \\ K_{ir}^{cT} & K_{rr}^c + K^b \end{bmatrix} \begin{Bmatrix} u_i^c \\ U_r^c \end{Bmatrix} = \begin{Bmatrix} F_i^c \\ F^* \end{Bmatrix} \tag{34a}$$

where

$$\{F^*\} = [C^b](\{\dot{\varepsilon}\} + \{\dot{U}_o^b\}) + [K^b](\{\varepsilon\} + \{U_o^b\} - \{U_o^c\}) \tag{34b}$$

If the bearing hydrodynamics are neglected, $\{\varepsilon\} = 0$. However even in this case, the crankshaft bent and block misboring produce equivalent forces according to Eq. (34b), which are applied on the crankshaft. All quantities in Eqs. (34a) and (34b) must be expressed in the rotating coordinate system.

Before Eq. (34a) are integrated in time to find the response of the reduced system, a torsional boundary condition is applied at the flywheel end of the crankshaft to eliminate the rotational free-body motion. For manual transmission applications or dynamometer tests, the torsional boundary condition consists of a torsional spring representing the propshaft torsional stiffness. For automatic transmission applications, a torsional damper boundary condition is used in order to capture the slipping of the torque converter.

Eqs. (34a) and (34b) are nonlinear since the nonlinear bearing hydrodynamics are implicitly involved through the bearing eccentricity vector $\{\varepsilon\}$. A modified Newmark method [43] with a Newton–Raphson based iteration at each time step, is employed for the time integration of Eqs. (34a) and (34b). At each time step, the following iteration loop is considered:

Step 1: Assume the bearing eccentricity vector $\{\varepsilon\}$.

Step 2: Calculate the bearing reaction forces and moments $\{F^b\}_{HYDRO}$ from the bearing hydrodynamics algorithm, using the assumed vector $\{\varepsilon\}$ from Step 1.

Step 3: Calculate the crankshaft retained displacement vector $\{U_r^c\}$ from Eqs. (34a) and (34b), based on the assumed $\{\varepsilon\}$.

Step 4: Calculate the block retained displacement vector $\{U_r^b\}$ from Eq. (31).

Step 5: Calculate the bearing reaction forces and moments $\{F^b\}$ from Eq. (24), based on the calculated $\{U_r^b\}$ from Step 4.

Step 6: If the absolute difference between $\{F^b\}$ and $\{F^b\}_{HYDRO}$ is greater than a small tolerance, update $\{\varepsilon\}$ and repeat the process from Step 1. Otherwise, proceed to the next time step.

The solution of Eqs. (34a) and (34b) gives the dynamic displacements of the reduced crankshaft–engine block system model. The displacements of the original crankshaft model can be obtained by two backwards

transformations (one for each level of substructuring). The displacements of the original model can be subsequently processed to calculate the crankshaft operating dynamic stresses.

7. Selected results

7.1. Dynamic analysis of an in-line five-cylinder engine

In order to experimentally validate the accuracy of the proposed methodology, the dynamic analysis of a five-cylinder in-line (L5) engine crankshaft was performed using the finite-element based analytical tool CRANKSYM which implements the methodology presented in this paper. The response of the L5 crankshaft under wide-open-throttle (WOT) operating conditions was simulated and correlated with measurements.

Figs. 5 and 6 show the measured and computed angular vibrations of the L5 crankshaft, respectively in "waterfall" format. The torsional vibration amplitude in degrees is plotted for different engine orders and engine speeds. Note that the measured and simulated vibration amplitudes are peak-to-peak and single amplitude (half of peak-to-peak), respectively. There is a very good correlation between the simulated with CRANKSYM and the measured vibrations at all engine speeds except around 6200 rpm at 2.5 engine order where CRANKSYM's prediction is about 20% higher than the measurement. The difference is mainly due to two reasons. First, the inherent nonlinearity of the tuned torsional vibration absorber's elastomer and second the coupling between the absorber's inertia ring and the accessory drive components.

The behavior of the nonlinear tuned absorber is such that higher vibration amplitudes would decrease the stiffness and increase the damping of the elastomer. This change in the elastomer material properties with deformation results in a decrease of the crankshaft resonance frequency and an increase of the crankshaft damping. The conducted simulations did not consider the nonlinear effects of the tuned absorber elastomer and

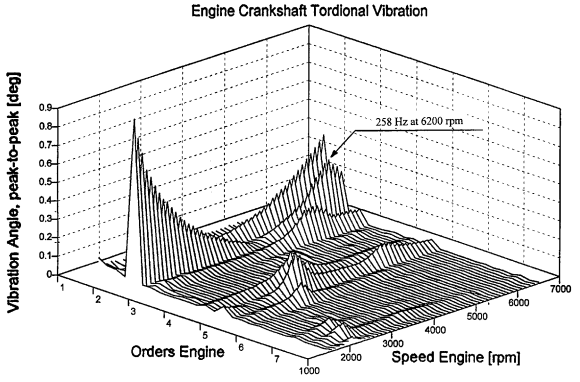

Fig. 5. Measured vibration for an in-line, five-cylinder engine.

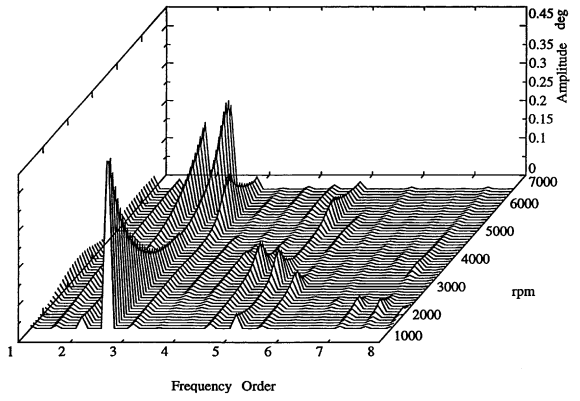

Fig. 6. Simulated vibration for an in-line, five-cylinder engine.

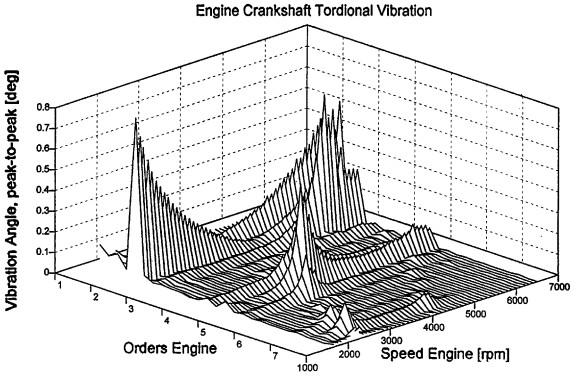

Fig. 7. Measured vibration for an in-line, five-cylinder engine with locked absorber's ring.

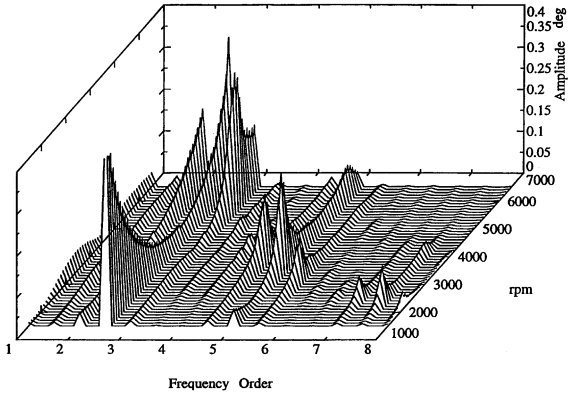

Fig. 8. Simulated vibration for an in-line, five-cylinder engine with locked absorber's ring.

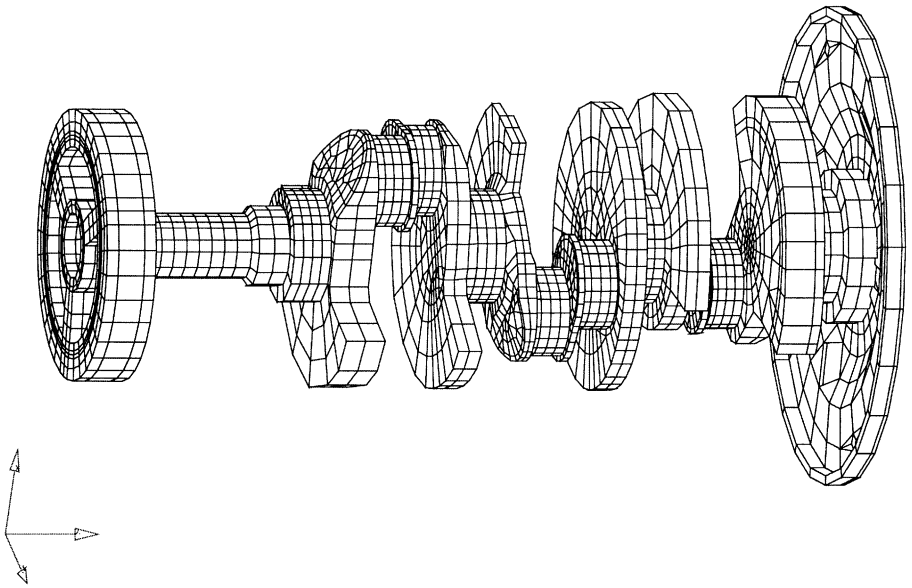

Fig. 9. The finite-element mesh for the pulley–crankshaft–flexplate system of the PV6 engine.

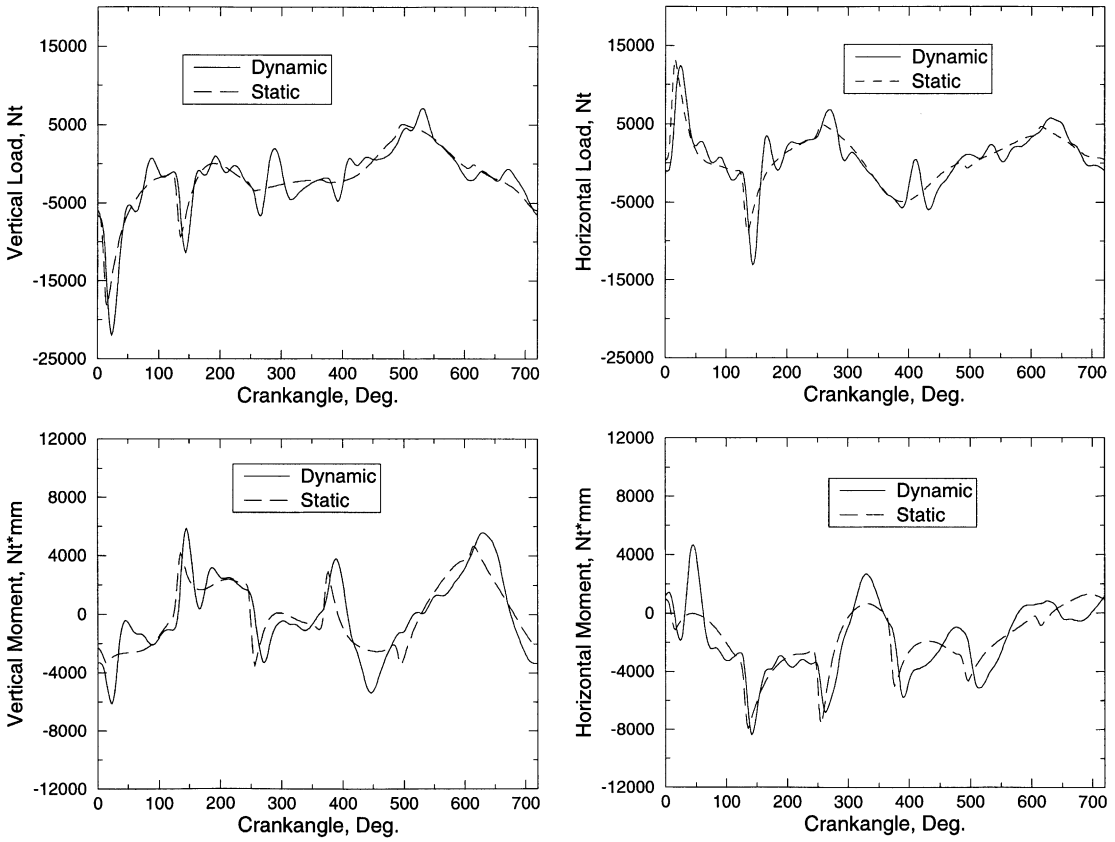

Fig. 10. Dynamic vs static calculation of bearing loads and moments.

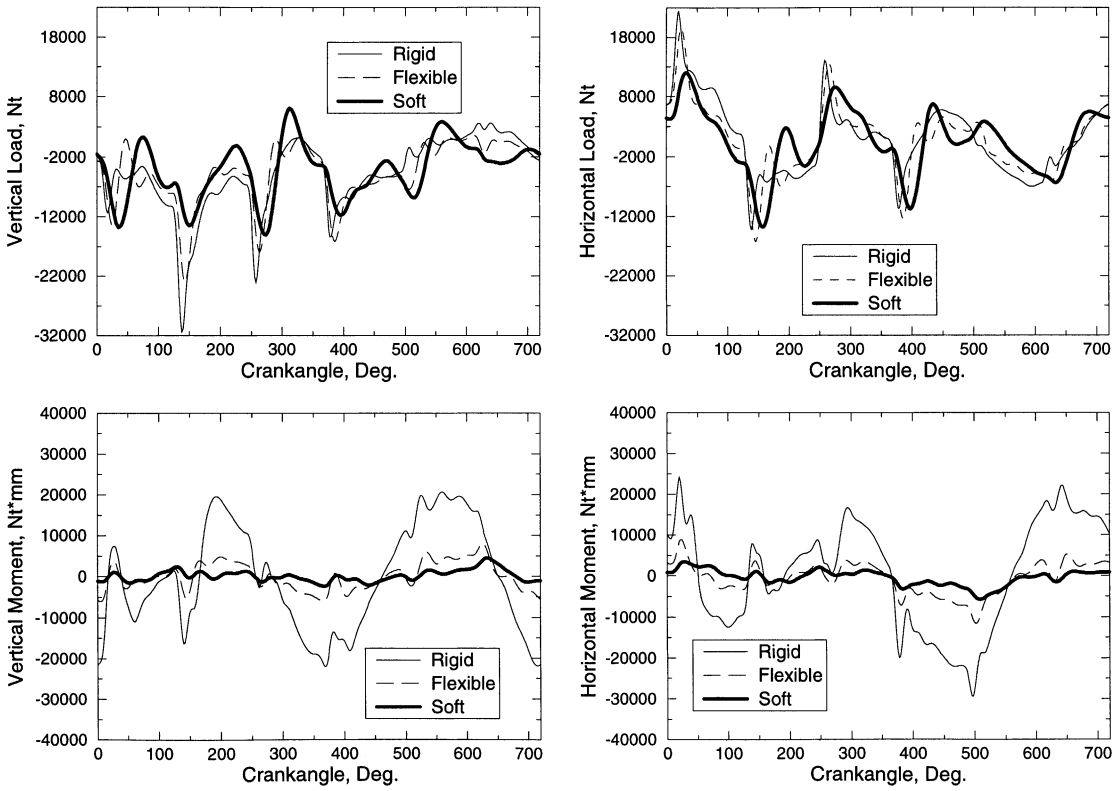

Fig. 11. Effect of block stiffness on bearing loads and moments.

therefore, such small differences between simulated and measured vibrations were expected.

The accessory drive components were found to interact with the tuned absorber's inertia ring since the latter is used as a pulley. This interaction seems to manifest itself as a decrease in the inertia of the ring which effectively increases the tuning frequency of the absorber. This inertia reduction effect was calculated and included in the simulations by decreasing the ring's inertia and increasing the tuning frequency of the absorber appropriately. The effect of the accessory drive components on the effective inertia of the absorber's ring can be significant and depends on which accessory components are present and whether A/C is engaged.

In order to eliminate the inherent nonlinearity of the tuned torsional vibration absorber's elastomer, the absorber's ring was pinned to the hub (locked ring) deactivating therefore, the effect of the elastomer's damping. Furthermore, the coupling between the absorber's inertia ring with the accessory drive components was eliminated by disconnecting the accessory drives from the crank pulley in a control dynamometer test. Figs. 7 and 8 show the measured and computed angular vibrations of the L5 crankshaft, respectively in this case. The agreement now is excellent. Note also that the peaks of the resonances are more pronounced since the absorber's damping is eliminated.

7.2. Dynamic analysis of a V6 (six-cylinder) engine

The V6 engine crankshaft, shown in Fig. 9, is used to demonstrate the capabilities of the proposed methodology and the importance of various design parameters in a crankshaft–block interaction study. Both the crankshaft pulley and the flexplate are included in the model. The finite-element mesh consists of 6814 solid elements and 8962 grids (26,886 degrees of freedom). The analysis was performed at 4500 rpm. Twenty Ritz vectors were used for both the first and the second substructuring. Both the combustion load and the inertia load due to reciprocating and rotating masses of the crank–connecting rod–piston assembly were considered in the calculation of the crankpin loads.

The effect of calculating bearing loads using a dynamic analysis as opposed to a static analysis is shown in Fig. 10. The vertical and horizontal loads as well as the vertical and horizontal bending moments are compared for the first bearing from the pulley end. A constant block stiffness of 100,000 N/mm in both the vertical and horizontal planes is used. As shown, the maximum

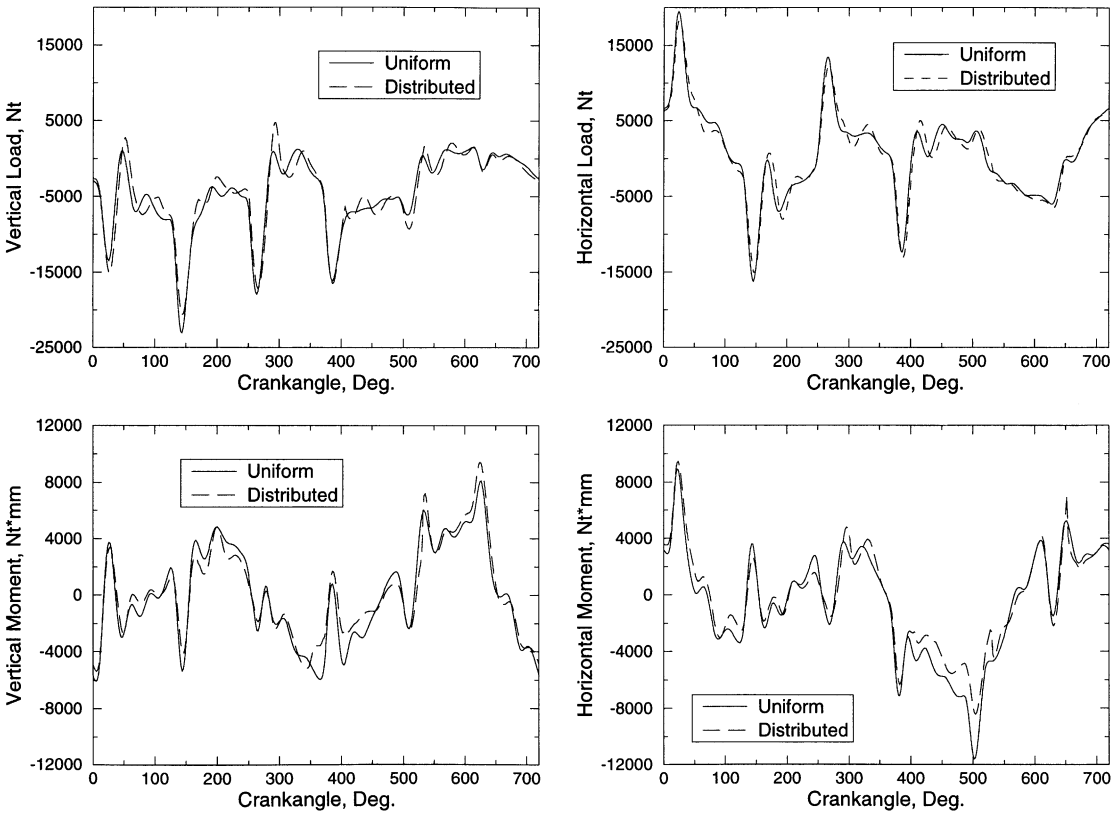

Fig. 12. Effect of circumferential block stiffness distribution on bearing loads and moments.

dynamic load is considerably higher than the maximum static load in both the vertical and horizontal planes. Substantial differences also exist in the vertical and horizontal bending moments. A large bending moment may generate a large journal misalignment which in turn, may alter the bearing hydrodynamic performance substantially.

Fig. 11 illustrates the effect of the block stiffness on bearing loads. The rigid, flexible and soft cases are compared for the second bearing. A 100,000 N/mm block stiffness is used for the flexible case which is representative of iron blocks. The block stiffness for the rigid and soft cases are 600,000 and 25,000 N/mm which are artificially large and small for the two respective cases. All stiffnesses were assumed circumferentially uniform for all bearings. The difference in both loads and moments, between the rigid and soft cases are substantial. This indicates the importance of the block stiffness in crankshaft dynamic analysis and clearly suggests the importance of the block dynamic behavior (not studied here).

The influence of engine block stiffness distribution around the bearing bore on the vertical and horizontal loads and moments is shown in Fig. 12 for the second bearing. The solid lines correspond to a uniform (not varying circumferentially) block stiffness of 100,000 N/mm. For the dashed lines, the block stiffness varies linearly between the values of 150,000 and 50,000 N/mm at the top (bulkhead) and bottom (bearing cap) locations of the bearing bore, respectively. The average of these two values is 100,000 N/mm which is representative of iron blocks. As shown in the figure, the circumferentially varying stiffness results in a maximum vertical load reduction of approximately 3000 N and a maximum horizontal moment reduction of approximately 4000 N mm.

Fig. 13 shows the effect of block misboring on the loads and moments of the fourth bearing. The misboring at each bearing location is arbitrarily defined by moving the third bearing upwards by 0.1 mm. All the other bearings are assumed to lie on a straight line. A constant block stiffness of 100,000 N/mm is used for all the bearings. The misboring distribution does not practically change the vertical and horizontal bearing loads. However, it drastically changes the bending moments. This suggests that the location of the bearing resultant loads is substantially moved along the bearing length. As a result, bearing end loading can occur with severe lubrication consequences and possible bearing failure. For this reason, any bearing misboring due to

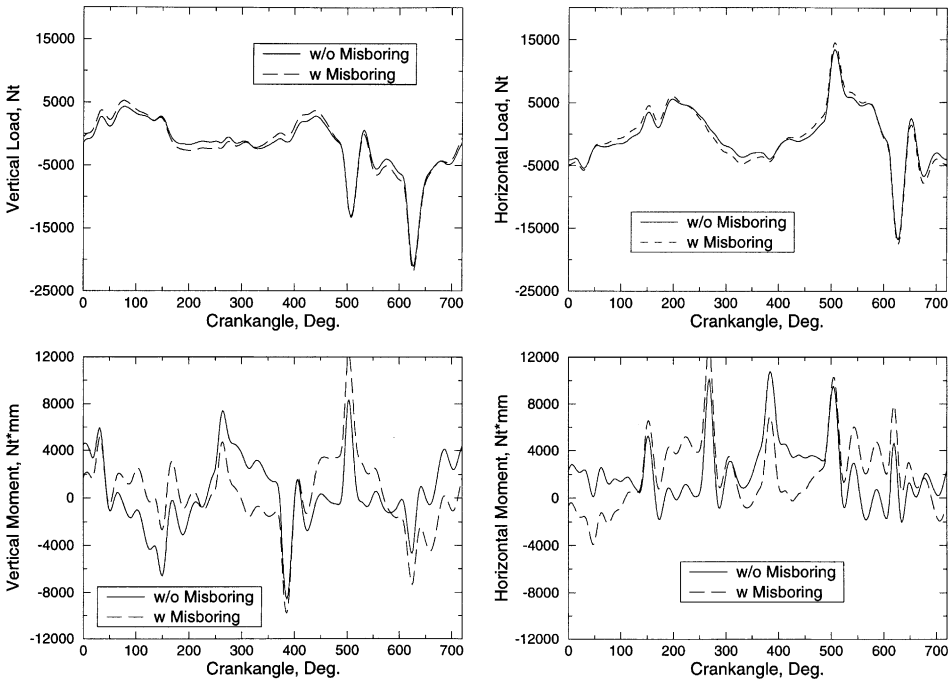

Fig. 13. Effect of block misboring on bearing loads and moments.

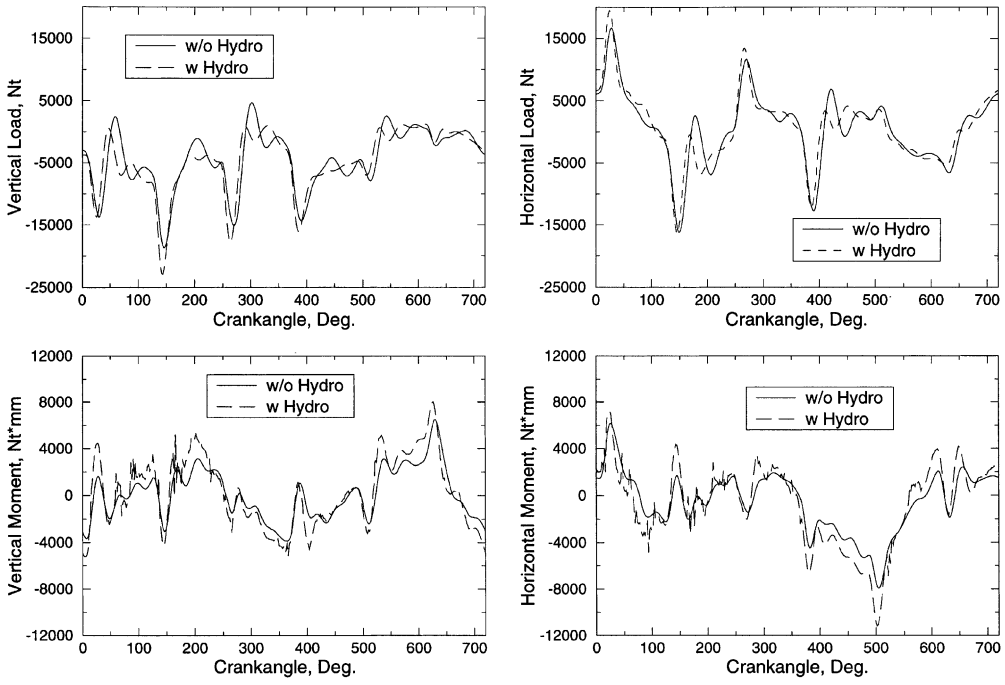

Fig. 14. Effect of bearing hydrodynamics on bearing loads and moments.

manufacturing imperfections should always be considered. Although results for the crankshaft bent are not presented here, it has been found having a similar to the block misboring effect.

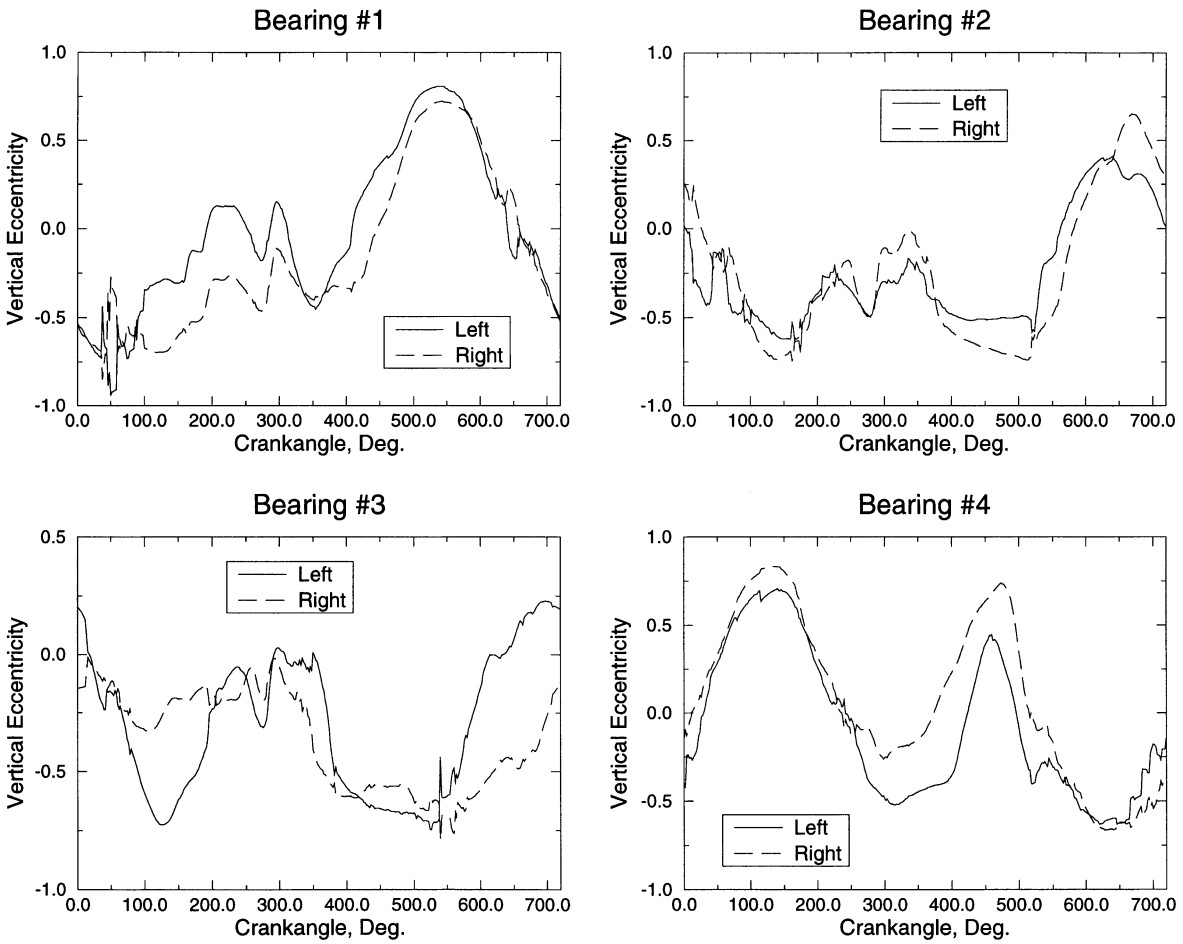

Fig. 15. Calculated journal misalignment in the vertical plane under dynamic loading.

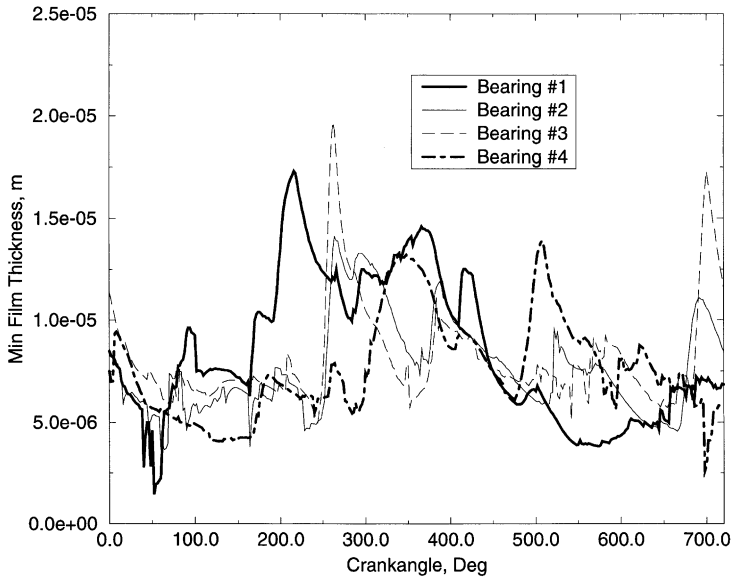

Fig. 16. Calculated bearing minimum film thickness under dynamic loading.

The effect of bearing hydrodynamics on the loads and moments of the second bearing is shown in Fig. 14. A 25 μm clearance is used for all bearings. A constant block stiffness of 100,000 N/mm is assumed. As shown in the figure, the inclusion of the bearing hydrodynamics in the analysis increased the maximum vertical load and the maximum horizontal moment considerably. Fig. 15 shows the vertical eccentricity for all four bearings at the left and right ends of the bearing. The difference between the left and right eccentricity indicates the amount of misalignment within each bearing. During most of the engine cycle, the bearing misalignment is considerable for all bearings. Since the misalignment can influence the hydrodynamic behavior of the bearing, it should be always considered when the bearing performance is assessed. Finally, Fig. 16 shows the minimum film thickness for all bearings. The minimum film thickness is around 5 μm for all bearings except the first bearing for which it is around 2 μm. This indicates that the bearings are not heavily loaded for this operating condition. For heavily loaded bearings, the minimum film thickness can be below 0.5 μm.

Acknowledgements

The author wishes to express his gratitude to Dr. Turgay Bengisu from the Synthesis and Analysis Department of the General Motors Powertrain Division for providing access to the experimental results presented in this paper. Furthermore, his efforts in productionizing and institutionalizing CRANKSYM within General Motors are greatly appreciated. His knowledge and experience on engine crankshaft vibrations and on vibrations in general have been invaluable in developing and improving CRANKSYM over the past few years.

References

[1] Henry JP, Toplosky J, Abramczuk M. Crankshaft durability prediction – a new 3-D approach. SAE paper no. 920087, 1992.

[2] Heath AR, McNamara PM. Crankshaft stress analysis – the combination of finite element and classical techniques. ASME ICE 1989;9.

[3] Kubota M, Kamichika R, Tanida K, Nakagawa E. Dynamic analysis of crankshaft using component mode synthesis. Part 1: efficient method of calculations utilizing NASTRAN image superelements. Bull Marine Engng Soc Jpn 1988;16(2).

[4] Mourelatos ZP. An analytical investigation of the crankshaft–flywheel bending vibrations for a V6 Engine. SAE International Proceedings of the 1995 Noise and Vibration Conference, vol. 1, SAE paper no. 951276, 1995.

[5] Kubozuka T, Hayashi Y, Hayakawa Y, Kikuchi K. Analytical study on engine noise caused by vibration of the cylinder block and crankshaft. SAE paper no. 830346, 1983.

[6] Ide S, Uchida T, Ozawa K, Izawa K. Improvement of engine sound quality through a new flywheel system flexibly mounted to the crankshaft. SAE paper no. 900391, 1990.

[7] Ochini K, Nakano M. Relation between crankshaft torsional vibration and engine noise. SAE paper no. 790365, 1979.

[8] Dejong R. Using vibration transmission analyses in the design of quiet engines. In: Hickling R, Kamal M, editors. Engine noise, excitation, vibration and radiation. New York: Plenum Press; 1982. p. 123–46.

[9] Welsh WA. Dynamic analysis of engine bearing systems. MS Thesis, Cornell University, 1982.

[10] Katano H, Iwamoto A, Saitoh T. Dynamic behaviour analysis of internal combustion engine crankshafts under operating conditions. Institute of Mechanical Engineers, Paper no. C430/049, 1991. p. 205–16.

[11] Nefske DJ, Sung SH. Coupled vibration response of the engine crank–block system. ASME 1989;DE-18-4:379–85.

[12] Mayer LS, Zeischka J, Scherens M, Maessen F. Analysis of flexible rotating crankshaft with flexible engine block using MSC/NASTRAN and DADS. 1995 MSC World Users' Conference, 1995.

[13] Martin IT, Law B. Prediction of crankshaft and flywheel dynamics. Institute of Mechanical Engineers, Paper no. C382/046, 1989.

[14] Law B, Haddock AK. Prediction of main bearing and crankshaft loading in reciprocating engines. 15th CIMAC Congress, Paris, 1983.

[15] Okamura H, Shinno A, Yamanaka T, Suzuki A, Sogabe K. A dynamic stiffness matrix approach to the analysis of three-dimensional vibrations of automobile engine crankshafts. Part I: background and application to free vibrations. ASME Winter Annual Meeting, Dallas, TX, 1990.

[16] Morita T, Okamura H. A dynamic stiffness matrix approach to the analysis of three-dimensional vibrations of automobile engine crankshafts. Part 2: application to firing conditions. ASME Winter Annual Meeting, Dallas, TX, 1990.

[17] Okamura H, Morita T. Influence of crankshaft–pulley dimensions on crankshaft vibrations and engine-structure noise and vibrations. SAE International Proceedings of the 1993 Noise and Vibration Conference. SAE paper no. 931303, 1993. p. 329–38.

[18] Stickler AC. Calculation of bearing performance in indeterminate systems. PhD Thesis, Cornell University, 1974.

[19] Booker JF. Dynamically loaded journal bearings: numerical application of the mobility method. Trans ASME, J Lubricat Technol 1971;93(1).

[20] Paranjpe RS, Cusenza A. FLARE: an integrated software package for friction and lubrication analysis of automotive engines. Part II: experimental validation. SAE Publication SP-919 on Engine Tribology, SAE paper no. 920488, 1992. p. 57–65.

[21] Goenka PK, Paranjpe RS. A review of engine bearing analysis methods at General Motors. SAE Publication SP-919 on Engine Tribology, SAE paper no. 920489, 1992. p. 67–75.

[22] Ishihama M, Hayashi Y, Kubozuka T. An analysis of the movement of the crankshaft journals during engine firing. SAE paper no. 810772, 1981.
[23] Mourelatos ZP. An efficient crankshaft dynamic analysis using substructuring with Ritz vectors. J Sound Vib 2000;238(3):495–527.
[24] Wilson EL, Yuan MW, Dickens JM. Dynamic analysis by direct superposition of Ritz vectors. Earthquake Engng Struct Dynam 1982;10:813–21.
[25] Arnold RR, Citerley RL, Chagrin M, Galant D. Application of Ritz vectors for dynamic analysis of large structures. Comput Struct 1985;21:461–7.
[26] Wilson EL, Bayo EP. Use of special Ritz vectors in dynamic substructure analysis. J Struct Engng 1986;112(8): 1944–54.
[27] Leger P, Wilson EL. Generation of load dependent Ritz transformation vectors in structural dynamics. Engng Comput 1987;4:309–18.
[28] Gockel MA, editor, MSC/NASTRAN: handbook for dynamic analysis. The MacNeal – Schwendler Corp., 1983.
[29] Reymond MA, editor, MSC/NASTRAN: User's manual. The MacNeal-Schwendler Corp., 1991.
[30] Bathe KJ, Wilson EL. Numerical methods in finite element analysis. Englewood Cliffs NJ: Prentice-Hall; 1976.
[31] Pinkus O, Sternlicht B. Theory of hydrodynamic lubrication. New York: McGraw-Hill; 1961.
[32] Brewe DE. Theoretical modeling of the vapor cavitation in dynamically loaded journal bearings. Trans ASME, J Tribol 1986;108:628–38.
[33] Paranjpe RS, Goenka PK. Analysis of crankshaft bearings using a mass conserving algorithm. STLE Tribol Trans 1990;33(3):333–44.
[34] Szeri AZ, editor. Tribology, friction, lubrication and wear. New York: Hemisphere; 1980.
[35] Cameron A. The principles of lubrication. New York: Wiley; 1966.
[36] Klit P, Lund JW. Calculation of the dynamic coefficients of a journal bearing, using a variational approach. ASME Paper 85-Trib-7. ASME/ASLE Joint Lubrication Conference, Atlanta, GA, October 1985.
[37] Goenka PK. Dynamically loaded journal bearings: finite-element method analysis. Trans ASME, J Tribolo Series F 1984:429–39.
[38] Mourelatos ZP, Parsons MG. Finite-element analysis of elastohydrodynamic stern bearings. SNAME Trans 1985; 93:225–59.
[39] Belytschko T, Liu WK, Kennedy JM. Hourglass control in linear and nonlinear problems. In: Alturi S, Perrone N, editors. Computer methods for nonlinear solids and structures, vol. 54, ASME/AMD. American Society of Mechanical Engineers, New York, 1983. p. 37–63.
[40] Kikuchi N. Finite element methods in mechanics. Department of Mechanical Engineering, The University of Michigan, 1985.
[41] Karni ZH, Parsons MG, Mourelatos ZP. Time-varying behavior of a statically indeterminate shafting system in a hydrodynamic journal bearing. ASME J Tribol 1987; 109(1).
[42] Mourelatos ZP. An efficient oil film lubrication analysis for engine crankshafts. Tribology Transactions 2001;44(3): 351–58.
[43] Newmark NM. A method of computation for structural dynamics. Proceedings of the American Society of Civil Engineers, 1959.